International Journal of Mass Spectrometry 273 (2008) 35–47

Contents lists available at ScienceDirect

International Journal of Mass Spectrometry

journal homepage: www.elsevier.com/locate/ijms

Scattering of very slow (3–10 eV) hydrocarbon ions CD_3^+, $CD_4^{\bullet+}$, and CD_5^+ from room-temperature carbon (HOPG) surfaces

Andriy Pysanenko[a], Jan Žabka[a], Fabio Zappa[b], Tilmann D. Märk[b], Zdenek Herman[a,b,*]

[a] V. Čermák Laboratory, J. Heyrovský Institute of Physical Chemistry, v.v.i., Academy of Sciences of the Czech Republic, Dolejškova 3, 182 23 Prague 8, Czech Republic

[b] Institut für Ionenphysik und Angewandte Physik, Leopold-Franzens Universität Innsbruck, Techniker str. 25, 6020 Innsbruck, Austria

ARTICLE INFO

Article history:
Received 13 December 2007
Received in revised form 19 February 2008
Accepted 19 February 2008
Available online 23 February 2008

Keywords:
Ion–surface scattering
Low energy collision
C1 hydrocarbon ions
Carbon surface

ABSTRACT

Scattering of simple hydrocarbon ions CD_3^+, $CD_4^{\bullet+}$, and CD_5^+ from room-temperature carbon (HOPG) surfaces was investigated at low incident energies of 3–10 eV. Mass spectra, angular and translational energy distributions of the product ions were determined. From these data, information on processes at surfaces, absolute ion survival probabilities, scattering diagrams, and effective mass of the surface involved in the collisions was determined. Incident ions CD_3^+ and CD_5^+ showed inelastic non-dissociative (CD_3^+) or non-dissociative and dissociative (CD_5^+) scattering, the radical cation $CD_4^{\bullet+}$ exhibited both inelastic, dissociative, and reactive scattering, namely occurrence of H-atom transfer and C-chain build-up in reactions with hydrocarbons present on the room-temperature carbon surface. The absolute survival probability, at 10 eV and the incident angle of 30° (with respect to the surface), was about 12% for CD_5^+, and 0.3–0.4% for CD_3^+ and $CD_4^{\bullet+}$. It decreased towards zero at lower incident energies. Estimation of the effective surface mass involved in the collisional process led to $m(S)_{eff}$ of about 29 a.m.u. for CD_3^+ collisions, to 15–21 a.m.u. for inelastic and fragmenting collisions of $CD_4^{\bullet+}$, and 62 a.m.u. for CD_5^+ collisions, corresponding roughly to the mass of one or several CH_3– (or C_2H_5–) terminal units of surface hydrocarbons. For the surface reaction of H-atom transfer in $CD_4^{\bullet+}$ collisions, the effective mass $m(S)_{eff}$ was about 48 a.m.u. suggesting a more complicated surface process than a simple direct H-atom pick-up reaction.

1. Introduction

Collisions of hyperthermal ions with surfaces have developed recently into a branch of research of interest to both physicists and chemists. Investigation of selected physical and chemical processes induced by impact of ions of energies below 100 eV has found over the last two decades many applications [1–6] ranging from surface diagnostics and surface modifications to characterization of projectile ions. Surface-induced activation and fragmentation of projectile ions has been used as one of the methods for characterizing structural properties of polyatomic ions ranging from relatively simple ions [7–9] to large biomolecules [10–13]. In particular, activation of biomolecular ions via surface collisions and the question of energy transfer associated with it has attracted considerable attention of both experimentalists and theoreticians [11–18]. Ion–surface collisions can be an important source of information relevant to plasma–wall interactions in fusion systems [5].

In our earlier papers we reported on studies of energy partitioning in collisions of low energy (15–50 eV) polyatomic ions with room-temperature stainless steel surfaces [6,19] and surfaces covered by self-assembled monolayers (SAM) [6,20], and room temperature and heated surfaces of carbon [6,21,22]. Fractions of incident energy resulting in internal excitation of the projectile, kinetic energy of product ions and energy absorbed by the surface were determined as a function of incident energy, incident angle, and type of the surface.

More recently, our work concentrated on collisions of low-energy small hydrocarbon ions with room temperature and heated carbon surfaces [21–24]. Motivation for these studies came from fusion research and urgent demand for data on collisions of low-energy (1–100 eV) simple hydrocarbon ions C1–C3 with room temperature and heated surfaces relevant for construction of fusion vessels (carbon, tungsten, beryllium). The projectile ions investigated were polyatomic ions hydrocarbon ions CH_n^+ (n = 3–5) and their isotopic variants [21], $C_2H_n^+$ (n = 3–6) and deuterated variants [23], cations and dications from toluene, $C_7H_n^{2+/+}$ (n = 6–8) [24]. The incident energy range was 15–50 eV. Mass spectra, translational

* Corresponding author at: V. Čermák Laboratory, J. Heyrovský Institute of Physical Chemistry, v.v.i., Academy of Sciences, Dolejškova 3, CZ-182 23 Prague 8, Czech Republic. Tel.: +420 2 6605 3514; fax: +420 2 8658 2307.
E-mail address: zdenek.herman@jh-inst.cas.cz (Z. Herman).

1387-3806/$ – see front matter © 2008 Elsevier B.V. All rights reserved.
doi:10.1016/j.ijms.2008.02.011

energy and angular distributions of product ions were measured as a function of the incident energy and incident angle of the projectiles. These measurements made it possible to determine the ion survival probability, energy transfer in surface collisions, and fragmentation and chemical reactions at surfaces. In collisions with surfaces heated to or above 600° C only fragmentation of the projectile ions was observed. With surfaces at room temperature, chemical reactions with surface material were observed, in addition to projectile ion fragmentation. The most prominent surface chemical reaction was H-atom transfer to radical cation projectiles and, of lesser importance, C-chain build-up reactions (formation of C_2- and C_3-hydrocarbon ions in collisions involving C_1 ion projectiles, C_3-hydrocarbon ions in collisions involving C_2 radical cations) in reactions with surface hydrocarbons. The occurrence of these chemical reactions appears to be a sensitive indication of surface coverage with hydrocarbons.

In this communication we report on results of scattering of very slow hydrocarbon ions CD_3^+, $CD_4^{\bullet+}$, and CD_5^+ of energies 3–10 eV (incident angle 30° with respect to the surface) from room-temperature carbon (highly oriented pyrolytic graphite, HOPG) surfaces. Measuring in the region of incident energies of a few eV required modification of the apparatus, namely a better collimation of the incident beam and an improved detection of very small signals. Data on mass spectra, angular distributions and translational energy distributions at different scattering angles of the product ions provided detailed information on the elementary processes in collisions of these low-energy ions with the surface material. New data on ion survival probability, incident energy transformation, fragmentation and chemical reactions were obtained. Kinematic analysis of the scattering data provided information on the inelasticity of surface collisions and on the effective surface mass involved in these ion–surface processes.

2. Experimental

The experiments were carried out with the Prague beam scattering apparatus EVA II modified for ion–surface collision studies (Fig. 1). The application of the apparatus to the surface studies was described earlier [6,19–24]. In the present experiments, the projectile ions CD_3^+ and $CD_4^{\bullet+}$ were formed by bombardment by 80 eV electrons of deuterated methane CD_4 in a low-pressure ion source. For an effective CD_5^+ preparation (chemical reaction $CD_4^{\bullet+} + CD_4 \rightarrow CD_5^+ + CD_3^\bullet$ in the ion source) the ion source pressure was increased three to five times. Ions were extracted from the ionization chamber, accelerated to about 150–200 eV, mass analyzed by a 90° permanent magnet, and decelerated to the required energy in a multi-element deceleration lens. To achieve a better collimation of the low energy projectile ion beam, an additional collimation slit (0.4 mm × 1 mm) was installed 4 mm in front of the exit slit (0.4 mm × 1 mm) of the deceleration lens (for a detailed configuration, see Fig. 9 later on).

The resulting beam had an energy spread of 200 meV, full-width-at-half-maximum (FWHM), angular spread of 1.6°, FWHM, and geometrical dimensions of 0.4 mm × 1.0 mm when leaving the exit slit. At ±5° the beam intensity was by a factor of 10^{-5} smaller than at its angular maximum at 0°. The collimated beam was directed towards the carbon target surface under a pre-adjusted incident angle Φ_S (measured with respect to the surface plane). Ions scattered from the surface passed through a detection slit (0.4 mm × 1 mm), located 25 mm away from the target, into a stopping potential energy analyzer. After energy analysis the ions were focused and accelerated to 1000 eV into a detection mass spectrometer (a magnetic sector instrument), and detected by counting the ions reaching a Galileo channel multiplier. The pri-

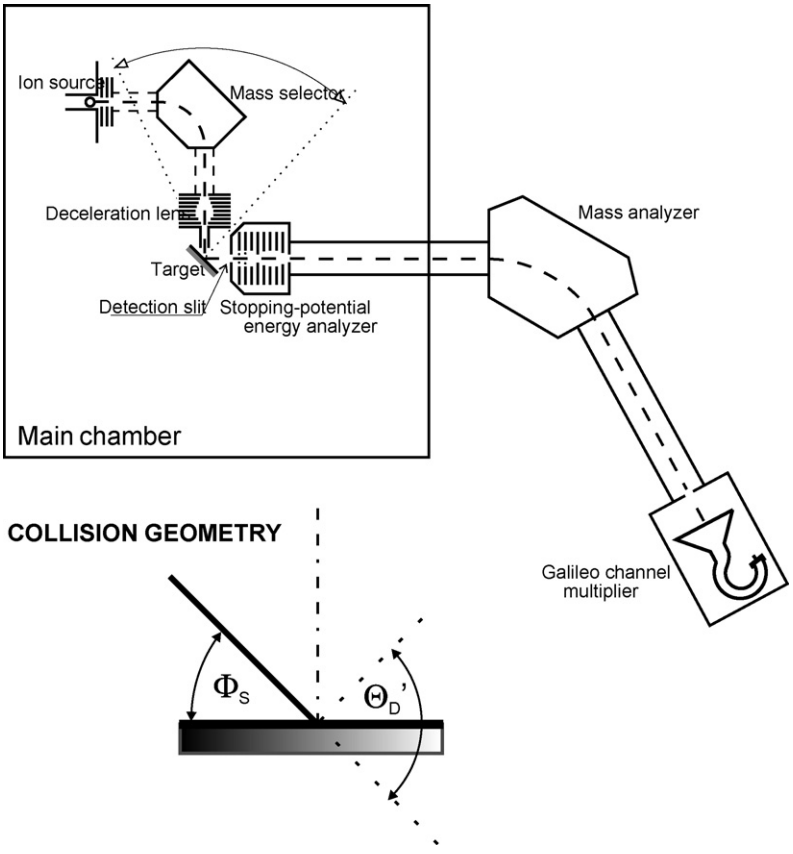

Fig. 1. Schematics of the ion–surface scattering apparatus. Inset defines the collision geometry.

mary beam exit slit, the target, and the detection slit were kept at the same potential during the experiments and this equi-potential region was carefully shielded by μ-metal sheets. The incident beam source–target section could be rotated about the scattering center with respect to the detection slit to obtain angular distributions. The mass spectra of product ions were recorded with the stopping potential set at zero, unless stated differently.

The nominal energy of the projectile ions was determined by the potential energy difference of the ionization chamber and the exit slit of the deceleration lens. The incident energy was determined in a special set of experiments, in which a stopping potential curve of the ion beam of a nominal energy incident on the HOPG surface located at the bottom of a Faraday cup was measured. It could be also measured in the arrangement as in Fig. 1 by applying to the target surface a potential exceeding the nominal ion energy by about 6 eV. The target area then served as a crude ion deflector directing the projectile ions into the detection slit located at about $\Theta'_D = 45^\circ$. The ion energy could be determined by the stopping potential energy analyzer with accuracy better than about 0.2 eV. The incident angle of the projectile ions in the experiments described here, Φ_S, was 30° (with respect to the surface plane). It was adjusted before an experimental series by a laser beam reflection with a precision better than 1°. Scattering angles (Θ'_D) were measured as a deflection from the original beam direction ($\Theta'_D = 30^\circ$ is the surface plane, see Fig. 1).

The carbon surface target was a 5 × 12 mm sample of highly oriented pyrolytic graphite (HOPG) from which the surface layer was peeled-off immediately before placing it into vacuum. The sample was mounted on a stainless steel holder located 10 mm in front of the exit slit of the projectile ion deceleration system. The carbon target surfaces in the experiments were kept at room temperature. It could be also resistively heated up to about 1000 K and its temperature measured by a thermocouple and/or by a pyrometer. The holder and heating jaws were located above and under the sample so that the scattering plane was free of any obstacles.

With carbon HOPG samples freshly placed into vacuum, a fraction of about 1% of the projectile ions of incident energies below 10 eV was found to be deflected with full energy in front of the surface due to impurities and local surface charges. Heating the samples to 1000 K for 60 min and subsequent cooling to room temperature led to lowering this deflected fraction of projectile ions to about 0.1% of the incident intensity and this fraction then practically did not change with time. Therefore, this treatment of new samples freshly put into vacuum was used as a standard procedure in preparation of samples for the experiments described in this study.

The scattering chamber of the apparatus was pumped by a 1380 l/s turbomolecular pump (Pfeiffer TMH 1600 M), and the detector by a 56 l/s turbomolecular pump (Pfeiffer TMH 065), both pumps were backed by rotary vacuum pumps. The background pressure in the apparatus was about 5×10^{-7} Torr, during the experiments the pressure was about 5×10^{-6} Torr due to the leakage of the source gas into the scattering chamber. Backstreaming of oil vapor from the rotary pump resulted, despite the installed molecular sieve trap, in covering the sample surfaces at room temperature with a layer of hydrocarbons in less than 1 h, as indicated by the occurrence of chemical reactions of H-atom transfer and C-chain build-up in the experiments with $CD_4^{\bullet+}$. Thus the HOPG surface at room temperature in the experiments described in this communication was always covered with a layer of hydrocarbons (backstreaming pump oil). It was shown earlier [20] that the surface with randomly adsorbed hydrocarbons behaved in energy transfer and reactivity very similarly to a hydrocarbon-SAM surface. Information on ion collisions with surfaces covered with hydrocarbons was a specific objective to complement the manifold of data for fusion research.

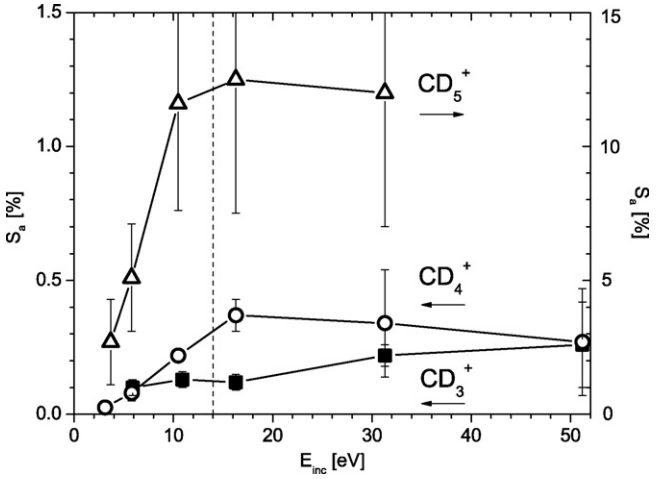

Fig. 2. Survival factors S_a (%) for CD_5^+, $CD_4^{\bullet+}$, CD_3^+ on room-temperature carbon (HOPG) as a function of the incident energy (incident angle 30° with respect to the surface). New data—points below 14 eV, earlier data (15–52 eV) from Ref. [21].

The projectile ion signal to the target surface could be measured directly by an electrometer when adjusting the projectile beam. The product ions reaching the Galileo multiplier of the detection mass spectrometer were counted. For the purpose of ion survival probability determination (see next paragraph), the count rates were transformed to ion currents.

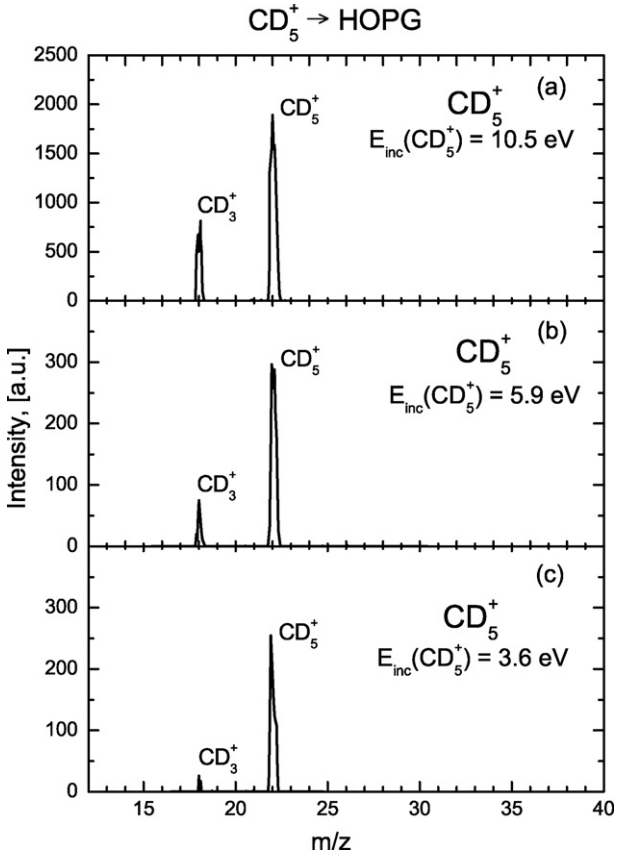

Fig. 3. Mass spectra of product ions from collisions of CD_5^+ with room-temperature HOPG surface at incident energy of (a) 10.5 eV, (b) 5.9 eV, and (c) 3.6 eV.

3. Results and discussion

3.1. Ion survival probability

The ion survival probability, S_a, is the percentage of ions surviving the surface collision. It is defined as the sum of intensities of all ions scattered from the target, ΣI_{PT}, to the intensity of the projectile reactant ions incident on the surface, I_{RT}, $S_a = 100\ \Sigma I_{PT}/I_{RT}$ (here, $I_{RT} = I_{RTM} + \Sigma I_{PT}$, where I_{RTM} is the current of projectile ions actually measured on the target). The quantities measured directly in our experiments were I_{RTM}, and the ion currents of product ions reaching the detector, ΣI_{PD} (sum of intensities in the mass spectrum of the product ions). The equivalent current of all product ions scattered from the target surface, ΣI_{PT}, had to be estimated from ΣI_{PD}, the discrimination of the apparatus (D_A), and the angular discrimination of the scattering differential measurements $D(\omega)_P/D(\omega)_R$, where $D(\omega)_P$ is the angular distribution of the product ions, $D(\omega)_R$ that of the reactant ions. The procedure used in the estimation of S_a was described in detail in our previous paper [21]. It leads to an expression for the absolute survival probability $S_a = 100FS_{eff}$, where the effective survival probability, $S_{eff} = \Sigma I_{PD}/I_{RT}$, contains the measurable quantities and the constant F summarizes all discrimination effects.

The discrimination effects of the apparatus were estimated as the ratio of the ion current entering the detection slit, I_{RS}, to the ion current reaching the detector, I_{RD}, $D_A = I_{RS}/I_{RD} = 2.0 \times 10^2$. The angular discrimination factor, $D(\omega)_P/D(\omega)_R$, was approximated by the squared ratio of the mean width (FWHM) of the product ion angular distribution, Ω_P(FWHM), to the acceptance angle of the detection slit, Ω_{DS}, $D(w)_P = \Omega_P^2/\Omega_{DS}^2$, and the analogous value for the reactant ion angular distribution (Ω_R), $D(w)_R = \Omega_R^2/\Omega_{DS}^2$. This gives $D(w)_P/D(w)_R = \Omega_P^2/\Omega_R^2$. The constant F in the present measurements was then $F = D_A[D(\omega)_P/D(\omega)_R]$; for Ω_R(FWHM) = 1.6° (see above) was $F = 78\Omega_P^2$, where Ω_P^2 was the square of the product ion angular distribution (FWHM) as determined from the angular distribution measurements.

The values of the survival probability of ions from collisions of CD_3^+, $CD_4^{\bullet+}$, and CD_5^+ with room-temperature carbon surfaces (incident angle $\Phi_S = 30°$) are given in Fig. 2 as a function of the incident energy. In addition to new values of S_a measured in this study for incident energies below 15 eV, earlier measured values of S_a [21] for incident energies 15–45 eV are given in the figure. It is encouraging that the old and new values of S_a agree with one another reasonably well, though obtained under rather different experimental conditions (different collimation of the reactant beam in this study and in [21], different detection systems: ion counting in this study vs. measurement of amplified analogue signals of product ions at the output of the electron multiplier in [21]).

The data in Fig. 2 show that the ion survival probability of the C1 cations for the incident angle of 30° (with respect to the surface) decreased toward zero at incident energies below 10 eV. The values of S_a for the close-shell cation CD_5^+ remained rather high, about 12% for incident energies above 10 eV and then decreased to about 3% close to 4 eV. The values of S_a for the open-shell, reactive cation $CD_4^{\bullet+}$ decreased from about 0.3–0.4% at incident energies

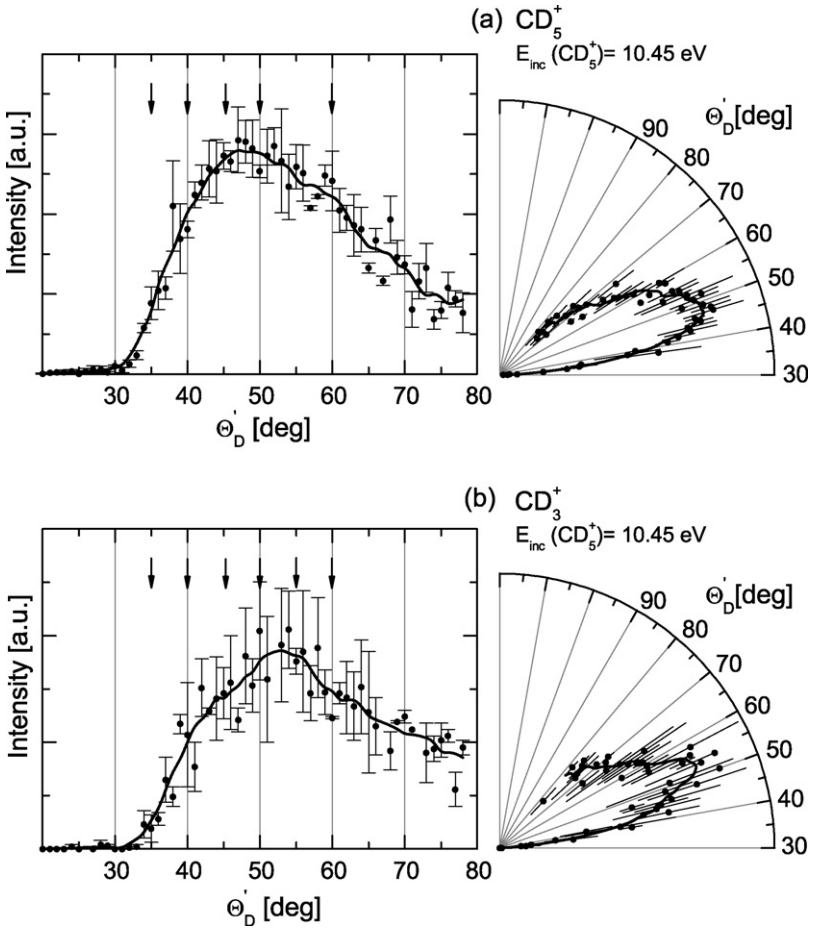

Fig. 4. Angular distributions and their polar plots (right) of product ions CD_5^+ (a) and CD_3^+ (b) from collisions of CD_5^+ of 10.45 eV. Translational energy distributions (Fig. 6) were measured at angles indicated by vertical arrows.

above 15 eV and the values of S_a for CD_3^+ were of the same order of magnitude.

The data on ion survival probability show that the most important process in the ion–surface collisions studied was incident ion neutralization. Therefore, it should be noted that when scattering of surviving ions is described below, the fate of only a minor part of the products is followed. The neutralized products may be scattered as neutral particles, they may react with the surface material to stable products (if neutral radicals are formed [25]), or they or their constituents (like D_2 [26]) may be embedded into the surface.

3.2. Scattering of projectile ions

Results of scattering measurements, namely mass spectra, angular and translational energy distributions of product ions, will be treated separately for the particular incident ions CD_3^+, $CD_4^{\bullet+}$, and CD_5^+.

3.2.1. CD_5^+

Scattering data for the projectile ion CD_5^+ seemed to be most straightforward to interpret of all three studied projectiles. The ion CD_5^+ is a closed-shell cation and its survival probability (several percent even at the lowest incident energies measured) is rather high, up to about 50-times higher than that or the projectile ions CD_3^+ and $CD_4^{\bullet+}$ (see Fig. 2). Fig. 3 summarizes mass spectra of product ions at collision energies of 10.5 eV, 5.9 eV, and 3.6 eV, respectively (for simplicity we refer to all ions scattered from the surface as product ions including CD_5^+, by composition the incident ion, however inelastically scattered). The only fragmentation process observed was dissociation of the incident projectile ion

$$CD_5^+ \rightarrow CD_3^+ + D_2 \quad (1)$$

The extent of this fragmentation decreased with decreasing collision energy from about 30% of the total product ion yield at 10.5 eV to about 10% at 3.6 eV. The energy defect of reaction (1) is thermodynamically 1.95 eV [27]. However, the reaction of D_2 loss from CD_5^+ is a rearrangement process and its activation energy was measured (1.1–1.4 eV [28]). Because only a fraction of the incident energy is converted to internal energy of the projectile ion in a surface collision [19–21], initial internal energy of the projectile ion presumably contributes to the extent of fragmentation at these low incident energies.

Fig. 4a and b shows the measured angular distributions of the product ions CD_5^+ and CD_3^+ at the collision energy of 10.45 eV as a function of Ω'_D. The right panels display polar plots of the measured data. Downward pointing arrows mark the scattering angles at which the translational energy distributions were measured. The angular distributions of both product ions were rather similar within experimental error, rising from the surface plane ($\Theta'_D = 30^\circ$) to a peak at about Ω'_D of 48–52° and decreasing afterwards. Fig. 5a and b shows angular distributions of the product ion CD_5^+at collision energies of 5.9 eV and 3.6 eV. There was a slight shift of the angular maximum towards larger Θ'_D (52° and 58° at 5.9 eV and 3.6 eV, respectively) with decreasing incident energy. A small intensity at about $\Theta'_D = 30^\circ$ and below was attributed to the contribution of background gas-phase scattering of the incident ion as discussed later on.

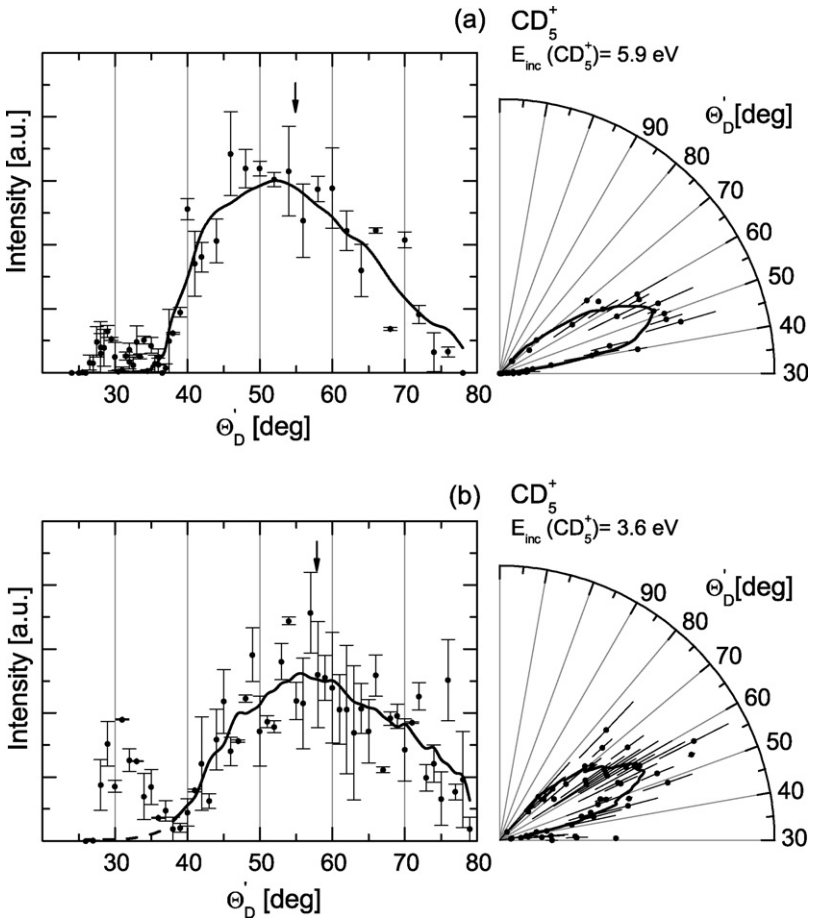

Fig. 5. Angular distributions and their polar plots of the product ion CD_5^+ at (a) 5.9 eV and (b) 3.6 eV. Translational energy distributions (Fig. 7) were measured at angles indicated by vertical arrows.

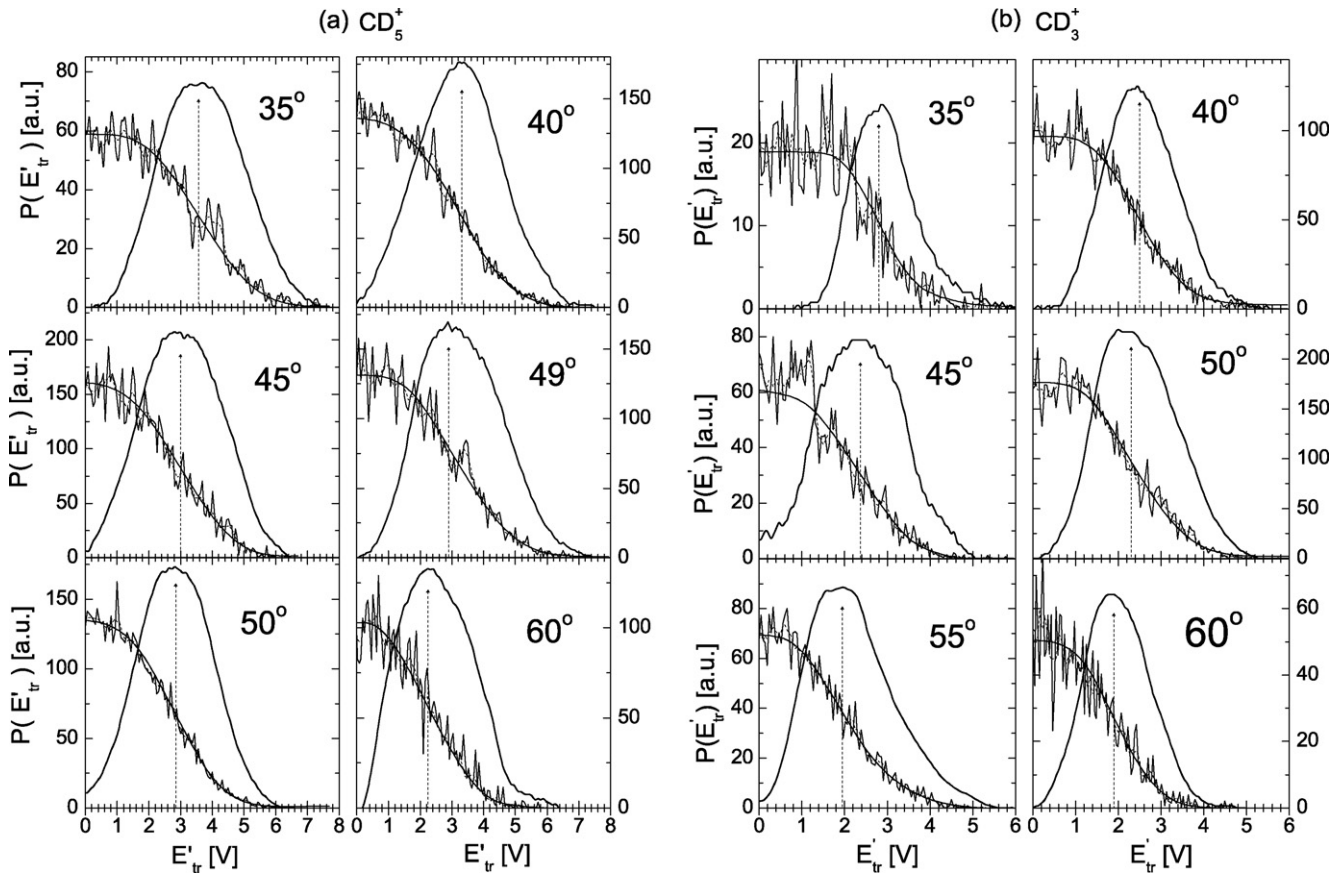

Fig. 6. Translational energy distributions of product ions (a) CD_5^+ and (b) CD_3^+ from collisions of CD_5^+ (10.45 eV) at a series of scattering angles between 35° and 60°. Figures show recorded stopping-potential curves (thin line), curves after 15-point smoothing (dashed), and smooth lines drawn through the latter.

Translational energy distributions of the product ions CD_5^+ and CD_3^+ at the incident energy of 10.45 eV are given in Fig. 6a and b for a series of scattering angles Θ'_D between 35° and 60°. The figures show the original stopping potential data (thin solid line) and the result of 15-point smoothing (dashed line). A smooth line was drawn through the data (thicker solid) and the translational energy distributions, $P(E'_{tr})$, were obtained as its derivative (solid line). The surface collisions were inelastic and the extent of inelasticity depended on the scattering angle. At the angular maximum the most probable translational energy was 30% of the incident energy. Fig. 7a and b gives the translational energy distributions of the undissociated product ion CD_5^+ at two incident energies of 5.9 eV (a) and 3.6 eV (b) measured at the angular maximum (see downward arrows in Fig. 5a and b). The translational energy distributions peaked at about 33 ± 1% of the incident energy.

3.2.2. CD_3^+

The projectile CD_3^+ is a fairly stable closed-shell ion that did not dissociate to fragments in the studied low-energy surface collisions. The thermodynamic limits of the dissociation processes are rather high, 3.5 eV and 5.5 eV for $CD_2^{\bullet+} + D^\bullet$ and $CD^+ + D_2$, respectively [27]. In the measured mass spectra, CD_3^+ was the only product ion observed at incident energies below 10 eV. Its survival probability was found to be about 50-times lower than that of CD_5^+(see Fig. 2). As a result, less probable phenomena and processes (negligible in the scattering of CD_5^+) were observed in the scattering data for CD_3^+. This can be seen in the angular distribution of CD_3^+ at the incident energy of 8.3 eV (Fig. 8). The angular distribution exhibited structures that resulted from overlap of different phenomena.

The peak at about 30° and stretching below this limiting value to about 26° (behind the plane of the sample) resulted from gas-phase elastic and inelastic scattering of the incoming projectile beam on background gas molecules (mostly CD_4 leaking from the ion source). This was confirmed by a series of special experiments to check this effect. The results were:

(i) introducing the second beam collimating slit (see Apparatus) led to narrowing of the half-width of the projectile ion beam as expected from geometrical considerations, but did not change significantly the tail of the beam in the vicinity of 30° and above it.
(ii) careful measurements of the shape of the projectile beam with the surface sample removed showed at scattering angles above 20° that the intensity was by about six-orders of magnitude smaller than the peak intensity, but comparable to that of the scattered product ion intensity for ions of survival factors below 1%, and depended linearly on the background pressure in the chamber. The shape of this gas-phase scattered profile was used in the applied corrections (see Fig. 8 and also Fig. 12).
(iii) increasing the length of the solid target shifted the cut-off at angles below 30° (surface plane) as expected from geometrical considerations (see Fig. 9).

The intense peak between 30° and 40° contained mostly projectile ions that had full incident energy. These fast ions appear to be projectile ions deflected in front of the surface by local surface micro-charges without making a surface collision at all. This phenomenon and the shape of the respective angular distribution was investigated in detail for $CD_4^{\bullet+}$ collisions and will be discussed there (see Fig. 12b). The intensity of this fraction of ions depended very much on the quality of the surface (see also Section 2). For new surfaces freshly introduced into vacuum it was about 10-times

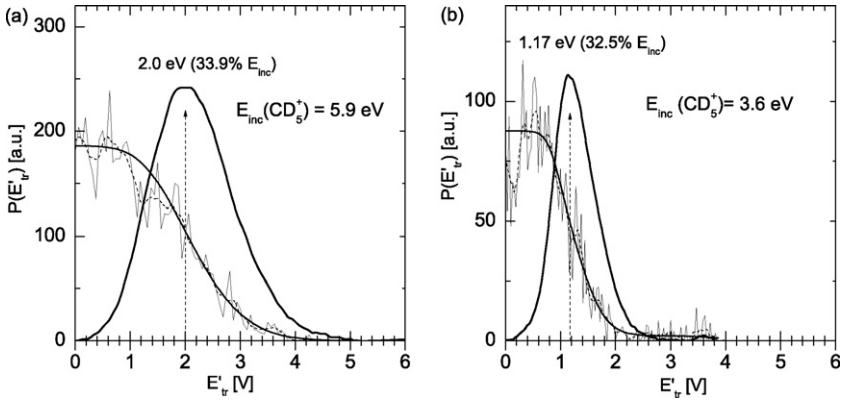

Fig. 7. Translational energy distributions of the product ion CD_5^+ at incident energies of projectile ion CD_5^+ of (a) 5.9 eV and (b) 3.6 eV close to the angular maximum.

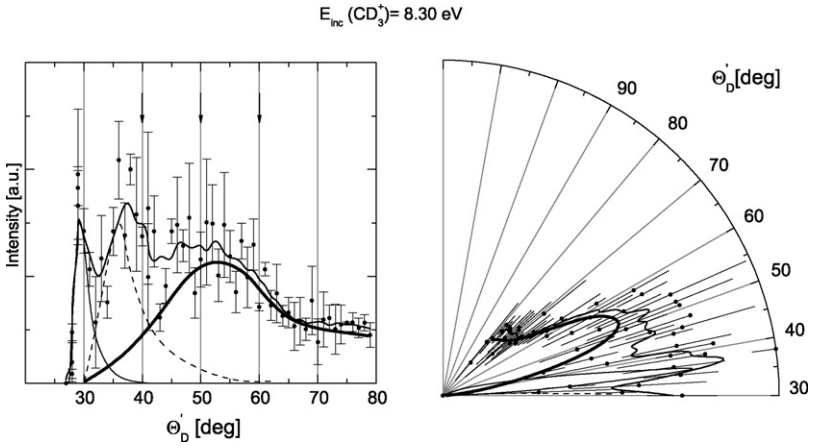

Fig. 8. Angular distribution and the respective polar plot of product ions CD_3^+ from CD_3^+ collisions with room-temperature HOPG surface at incident energy of 8.3 eV and its analysis: thin line and hatched, contribution of background gas-phase scattering; dashed, fast ion contribution; thick line, neat inelastic scattering.

larger than the intensity of the product ions from surface collisions. Heating of the surface in vacuum and subsequent cooling to room temperature to re-establish the surface hydrocarbon layer led to reduction of this fraction to about 10% of the original value. This effect became important on carbon surfaces only at very low incident energies below 10 eV. Angular distributions of these fast projectile ions were obtained from repeated measurements with the stopping potential set about 2–3 eV below the full energy of the incident ions and found to be – within experimental error – quite similar to enable a standard correction of the data. The angular distribution increased to a maximum a few degrees above the surface plane and then decreased rather quickly toward larger scattering angles (see Fig. 12b).

The measured angular distribution of CD_3^+ in Fig. 8 was corrected by subtracting these two contributions (gas-phase scattering and fast ion contribution) and it is shown by a solid line. It represents the net angular distribution of CD_3^+, inelastically scattered from the HOPG surface. Its shape was rather similar to that of inelastically scattered CD_5^+ in Figs. 3 and 5, increasing from 30° to a maximum at about 50° and decreasing afterwards.

Translational energy distributions of CD_3^+ measured at several scattering angles are given in Fig. 10. The distributions show a peak of inelastically scattered undissociated CD_3^+ ions and the contribution of fast projectile ions deflected by surface charges with full incident energy of 8.4 eV. The peak energy of the inelastically scattered CD_3^+ ions measured close to the angular maximum (at 50°) was 2.6 eV, i.e., 31% of the incident energy, similarly to the value obtained for the scattering of CD_5^+ ions.

3.2.3. $CD_4^{\bullet+}$

The projectile ion $CD_4^{\bullet+}$ is a radical cation that not only fragmented in surface collisions, but also chemically reacted with the surface material [21]. The mass spectra of reaction product ions thus contained contributions from the following processes (Fig. 11):

(a) inelastically scattered projectiles ion and products of its direct fragmentation after surface collision: ions $CD_4^{\bullet+}$, CD_3^+, and traces of $CD_2^{\bullet+}$ (open areas under the peaks in Fig. 11) from fragmentation processes (S for surface)

$$CD_4^{\bullet+} + S \rightarrow CD_3^+ + D^{\bullet} \quad (2)$$

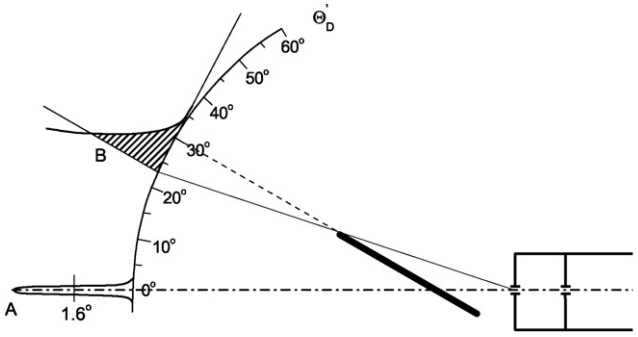

Fig. 9. Geometry for estimation of the range of background gas-phase scattering of projectile ions: projectile ion exit slits at right, dash-and-dot line, direction of the projectile beam with its angular distribution at 0° (A); thick line, target; dashed area, tail of gas-phase scattered projectile ion signal with a cut-off at B.

$$CD_4^{\bullet+} + S \rightarrow CD_2^{\bullet+} + D_2 \quad (3)$$

(b) products of H-atom transfer from hydrocarbons on the surface (hatched in Fig. 11); the reaction led to the formation of CD_4H^+ and its dissociation products (CD_3^+, CD_2H^+) in reactions

$$CD_4^{\bullet+} + CH_3{-}S \rightarrow CD_4H^+(+{}^{\bullet}CH_2{-}S) \rightarrow CD_3^+ + HD \quad (4a)$$

$$CD_4^{\bullet+} + CH_3{-}S \rightarrow CD_4H^+(+{}^{\bullet}CH_2{-}S) \rightarrow CD_2H^+ + D_2 \quad (4b)$$

(c) products of chemical reactions of carbon chain build-up with hydrocarbons on the surface (ions $C_2DH_2^+$ and $C_2D_2H^+$, observable only in Fig. 11a at the incident energy of 10.65 eV, hatched); these ions were shown earlier [21] to be final products of reactions between the projectile and the terminal group of surface hydrocarbons, namely

$$CD_4^{\bullet+} + CH_3{-}S \rightarrow C_2D_4H_3^+(+{-}S^{\bullet}) \rightarrow C_2X_5^+(+X_2) \rightarrow C_2X_3^+(+X_2) \quad (5)$$

where X denotes H or D.

(d) fast $CD_4^{\bullet+}$ projectiles deflected in front of the surface with full incident energy by charged insulating micro-islands (cross hatched in Fig. 11).

The mass spectra in Fig. 11 showed that with incident energy decreasing below 10 eV the extent of fragmentation decreased. The endoergicities [27] of processes (2) and (3) are 1.85 eV and 2.6 eV, respectively. The maximum energy expected to be converted in a surface collision into internal energy is only a fraction of the incident energy and thus, as in the case of CD_5^+ collisions, the extent of fragmentation of CD_4^+ is influenced by the initial internal energy of the projectile ions (see also fragmentation of relaxed and non-relaxed projectile ions CD_4^+ in Ref. [29]). Ions resulting from surface chemical reactions were formed and partially fragmented at the incident energy of 10.65 eV, where they represented a larger part of product ions formed (see hatched areas in Fig. 11a). At 6.05 eV only formation of non-dissociated CD_4H^+ was observed, and at 3.1 eV

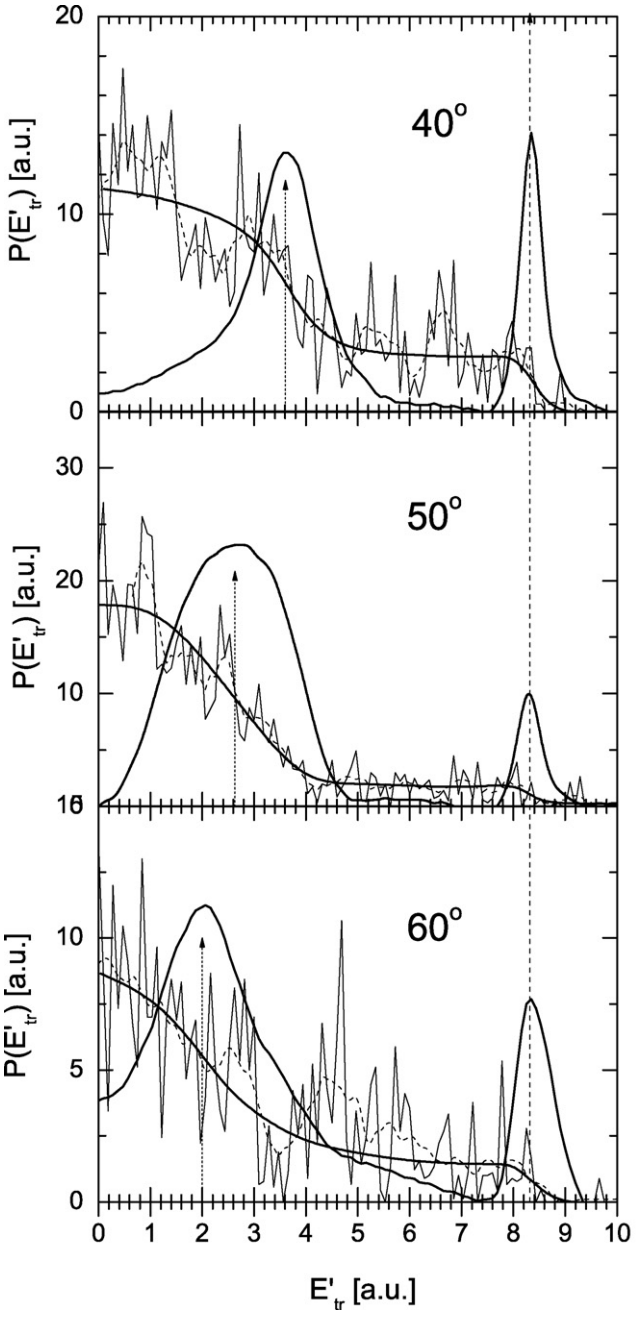

Fig. 10. Translational energy distributions of product ions CD_3^+ from collisions of CD_3^+ (8.3 eV) at three different scattering angles. Details as in Fig. 6.

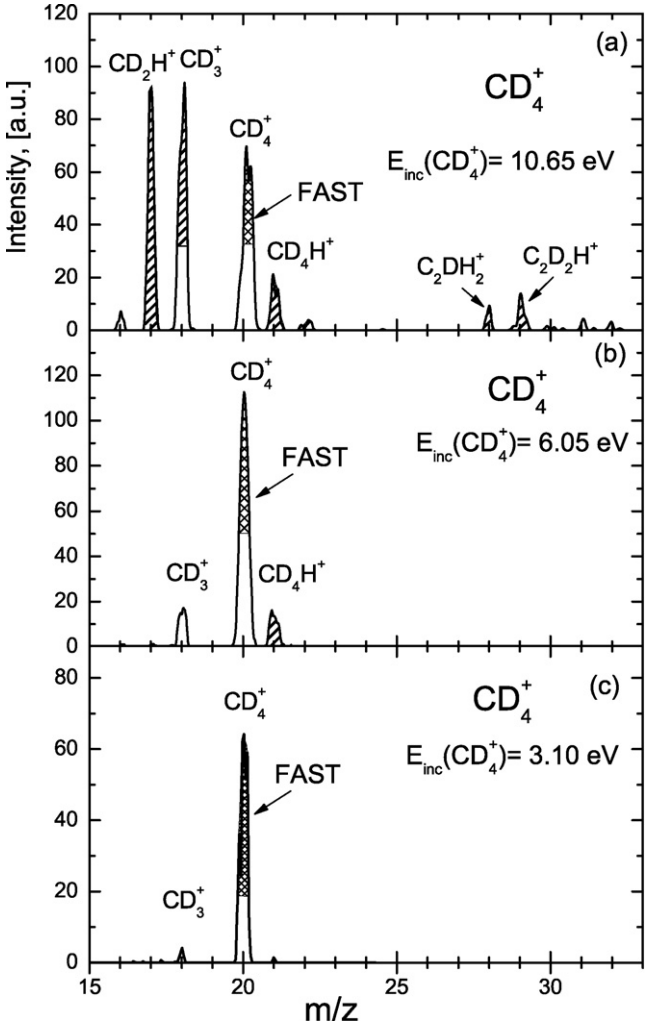

Fig. 11. Mass spectra of product ions from collisions of $CD_4^{\bullet+}$ with room-temperature HOPG surface at the incident energy of (a) 10.65 eV, (b) 6.05 eV, (c) 3.1 eV. Hatched area, contributions from chemical reactions; crossed hatched, fast ion contribution.

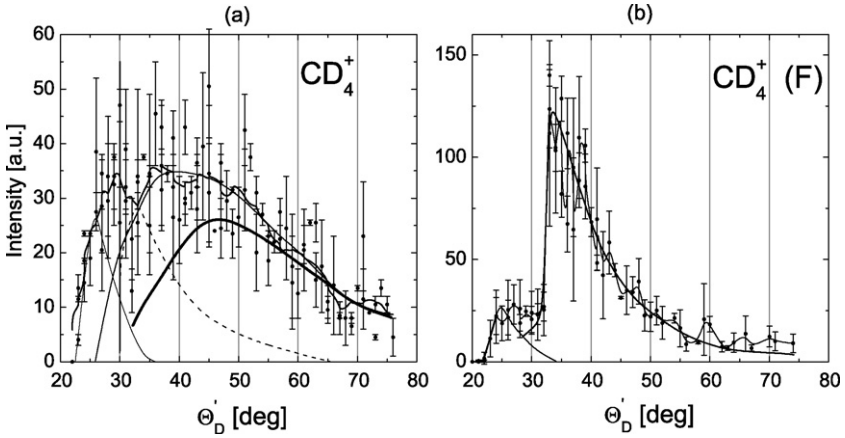

Fig. 12. Angular distribution of the product ion $CD_4^{\bullet+}$ from collisions of $CD_4^{\bullet+}$ at 10.65 eV (a) $CD_4^{\bullet+}$ scattering and its analysis (b) $CD_4^{\bullet+}$ fast ion component. Thin line and hatched, contribution of background gas-phase scattering; dashed, fast ion contribution; solid line, neat inelastic surface scattering.

formation of product ions from chemical reactions was below the limit of detection.

The survival probability of $CD_4^{\bullet+}$ projectile ions was less than 0.2% at incident energies below 10 eV (see Fig. 2), comparable to that of CD_3^+. Therefore, similar to CD_3^+, the measured angular distribution of $CD_4^{\bullet+}$ (Fig. 12a) had to be corrected for the gas-phase background scattering (hatched area) and for the contribution of fast projectile ions deflected with full energy in front of the target.

The angular distribution of this fast ion fraction was measured in separate experiments in which the potential of the stopping field of the analyzer was set at 8 V, about 2 eV below the incident energy. The resulting curve is shown in Fig. 12b. It shows a sharp increase from the surface plane to a maximum at about 34° and a gradual decrease towards larger scattering angles. A simulation of ion trajectories deflected by a single point charge on the surface was carried out using the SIMION program. In this simulation 20 eV ions were directed with the incident angle of 30° (with respect to the surface) and different impact parameters, to a point charge on the surface at a potential of +30 V. The angular distribution of deflected trajectories showed a peak at about 5–10° above the surface and a gradual decrease towards larger angles, a rather similar shape to the curve in Fig. 12b.

The data for $CD_4^{\bullet+}$ in Fig. 12a were then corrected by subtracting these two contributions (the relative contributions of gas-phase scattering and fast ion fractions in Fig. 12a and b cannot be directly compared, as they were obtained under different conditions). The resulting curve of $CD_4^{\bullet+}$ inelastic surface scattering is shown in Fig. 12a by a solid line raising from 30° to a peak at about 47° and decreasing afterwards. Though the scatter of data after both subtractions is quite large, the shape of the net inelastically scattered $CD_4^{\bullet+}$ curve is quite similar to that of the CD_5^+ inelastic scattering curve in Fig. 4a.

Fig. 13 summarizes data on angular distributions of other major product ions from $CD_4^{\bullet+}$ surface collisions, CD_3^+ and CD_2H^+. The ion CD_2H^+ was a net product of the surface chemical reaction followed by the fragmentation of CD_4H^+, reaction (4b). The current for CD_3^+ contained contributions from two processes, direct fragmentation of the inelastically scattered $CD_4^{\bullet+}$ projectile, reaction (2), and fragmentation of the chemical reaction product CD_4H^+, reaction (4a). In addition, the scattering of CD_3^+ had to be corrected for a background gas-phase dissociative scattering (collision-induced dissociation) of the projectile $CD_4^{\bullet+}$. Its shape and relative contribution was again determined by experiments without the solid target, and is shown in Fig. 13a as a hatched area. The remaining net inelastic CD_3^+ scattering may at least approximately be divided into the chemical reaction contribution, reaction (4a) (dashed in Fig. 13a) and the rest—direct fragmentation of the projectile ion, reaction (2) (dotted in Fig. 13a). The former contribution was obtained as the fraction (2/3) of the CD_3^+ peak height in the mass spectra at the angular maximum (Fig. 11a) and by copying the shape of the intensity-adjusted angular distribution of CD_2H^+ from Fig. 13b.

Data on translational energy distributions of the product ions $CD_4^{\bullet+}$, CD_3^+, and CD_2H^+ at the incident energy of $CD_4^{\bullet+}$ at different scattering angles are given in Fig. 14. The data for $CD_4^{\bullet+}$

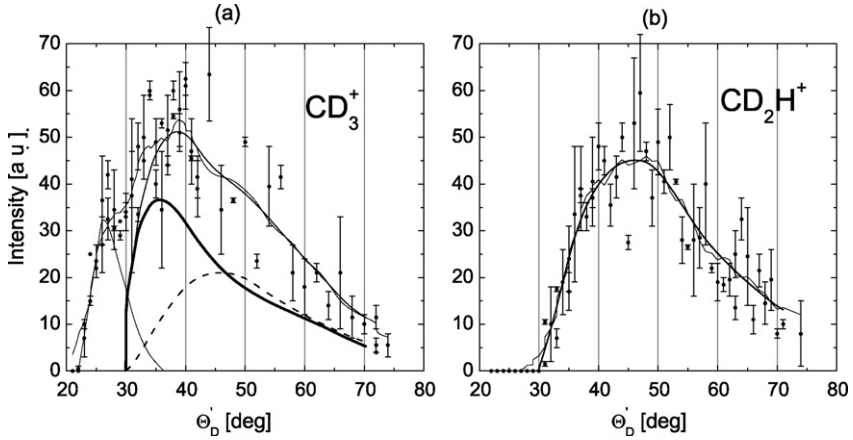

Fig. 13. Angular distribution of product ions (a) CD_3^+ and (b) CD_2H^+ from collisions of $CD_4^{\bullet+}$ at 10.65 eV and its analysis. Thin line and hatched, contribution of background gas-phase dissociative scattering; dashed, contribution of surface chemical reaction to CD_3^+; thick solid line, net contribution of dissociative surface scattering.

showed both the inelastic scattering of non-dissociated $CD_4^{\bullet+}$ (peaks at 5.5 eV or at 3.2 eV) and the contributions of fast $CD_4^{\bullet+}$ ions deflected in front of the surface with full incident energy (10.65 eV) by surface micro-charges. The translational energy data for CD_3^+ showed two inelastic peaks, the relative contribution of the peak at higher energy decreased with increasing scattering angle. Translational energy distributions for the chemical reaction fragmentation product CD_2H^+ peaked at a single energy, decreasing slowly with increasing scattering angle.

3.3. Kinematic analysis of the scattering data

The data on angular and translational energy distributions of inelastically and reactively scattered product ions from collisions of CD_5^+, CD_3^+, and $CD_4^{\bullet+}$ (Figs. 4–14) were used to construct velocity contour scattering diagrams of these ions. Similar analyses were carried out earlier for inelastic and reactive scattering of hyperthermal neutral O and Cl atoms from hydrocarbon (squalene) surfaces [30,31]. The scattering data from ion–surface collisions were treated as in gas-phase scattering [32,33]. Translational energy distributions of product ions were converted to velocity distributions (Cartesian probability plots) and normalized to the intensity in the angular distribution at a particular angle.

In Fig. 15a, the normalized velocity distributions of CD_5^+ were plotted as contours against the scattering angle Θ'_D (data from Figs. 4 and 6a). The arrow on the left hand side indicates the incident angle (30° with respect to the surface) and v_{inc} represents the velocity of the incident projectile ion CD_5^+ (9.58 km/s for E_{inc} = 10.45 eV) plotted from the impact point on the surface (0). For a surface target element fixed on the surface ($v_s = 0$), $v_{inc}(CD_5^+)$ also represents the relative velocity, v_{rel}, of the projectile of known mass ($m(CD_5^+)$ = 22 a.m.u.) with respect to the target element of an effective mass $m(S)_{eff}$. It can be seen that the local maxima in the velocity distributions fall on a circle of

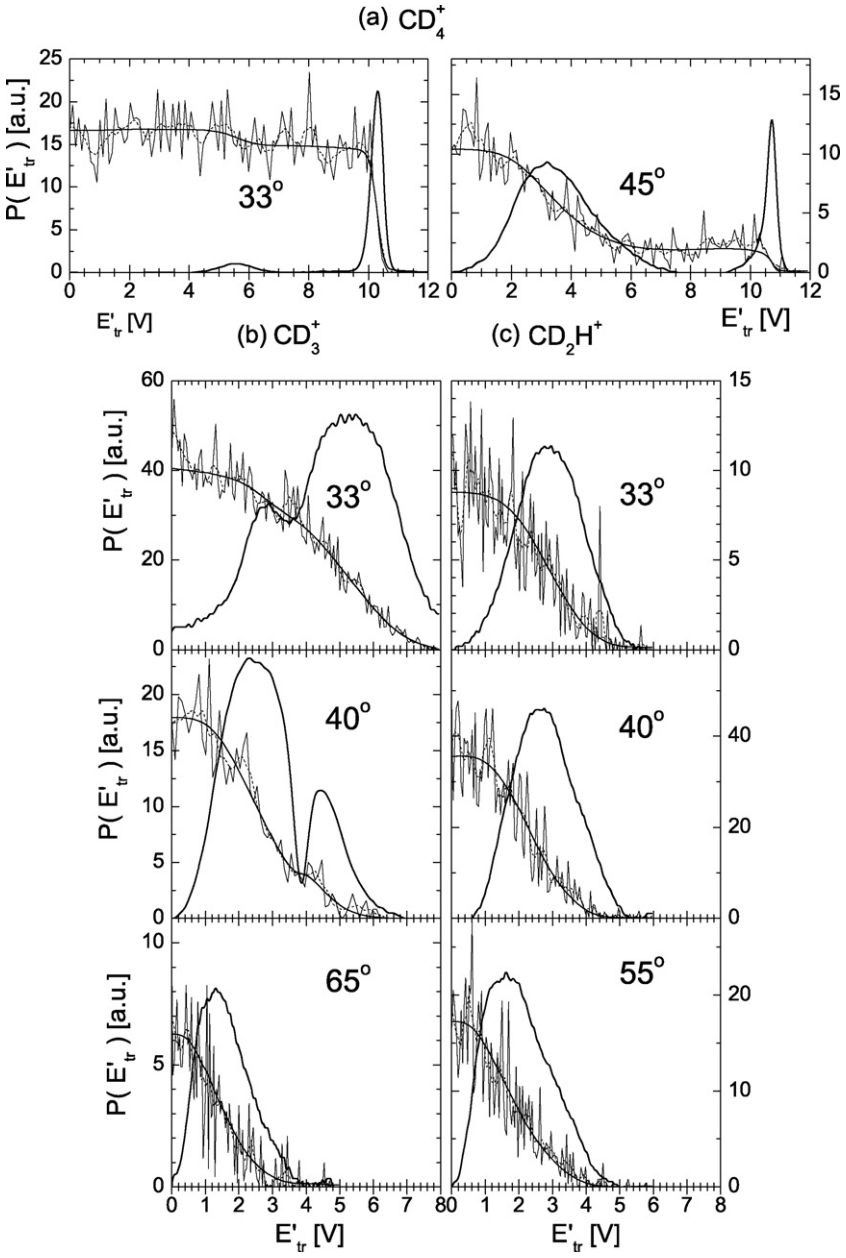

Fig. 14. Translational energy distributions of product ions from collisions of $CD_4^{\bullet+}$ at 10.65 eV: (a) $CD_4^{\bullet+}$ at 33° and 45°, (b) CD_3^+ at 33°, 40°, and 65°, (c) CD_2H^+ at 33°, 40°, and 55°. Details as in Fig. 6.

radius 3.80 km/s the center of which bisects the velocity at a point denoted CM, the effective center of mass of the colliding system of incident projectile ion-effective surface element. The respective components of this bisected relative velocity may be then regarded as the center-of-mass velocity of the projectile ion, $u(CD_5^+)$, and the center-of-mass velocity of the effective surface element, $u(S)$, and may be used to estimate the effective mass of the surface element involved in the collision, $m(S)_{eff} = m(CD_5^+)\ u(CD_5^+)/u(S)$. In this case $u(CD_5^+) = 7.08$ km/s and $u(S) = 2.5$ km/s and this led to the estimated effective mass of the surface involved in the collision, $m(S)_{eff} = 62$ a.m.u. On the carbon (HOPG) surface covered at room temperature with hydrocarbons this represented the mass of about two CH_3CH_2- terminal groups or about four CH_3- terminal groups of surface hydrocarbons.

The interpretation of the effective surface mass of the surface involved in the collision is, obviously, not straightforward. The scattering results provide an average picture of many collision events with different sites on surface which is not uniquely defined. However, we believe that it is a useful parameter to follow and to use to compare data for different incident ions on the same type of surface. In the above mentioned case of CD_5^+ collisions, the results of both inelastic (product CD_5^+) and dissociative (product CD_3^+) scattering, $m(S)_{eff}$ (62 a.m.u.) appears to be much larger than in case of CD_3^+ and partly CD_4^+ scattering (see later). It may indicate a surface process more complicated than a simple dissociation. It was noted earlier [28] that the gas-phase collisional activation and dissociation of CD_5^+ is a more complicated process presumably requiring isomerization and subsequent fragmentation.

The simplified scattering diagram in Fig. 15b shows only maxima of the velocity distributions of both product ions, CD_5^+ and its fragment CD_3^+ plotted at the particular scattering angles in the framework of the scattering diagram (data from Figs. 4 and 6). The data for both product ions lay on the same circle and led to the same conclusion concerning the effective mass of the surface involved in the collision. The similarity of the CD_5^+ and CD_3^+ translational energy (velocity) distributions also indicated that fragmentation of the inelastically scattered projectile ion took place *after* the interaction with the surface in the unimolecular way, a finding observed earlier for a series of different polyatomic projectile ions [6,19–23].

The simplified scattering diagram of product ions CD_3^+ from collisions of CD_3^+ with the carbon surface is shown in Fig. 16. Again, the peaks in the velocity distributions (obtained from translational energy data, Fig. 10) were plotted against the scattering angle. The velocity peaks fitted on a circle with a radius of 4.15 km/s the center of which bisected the relative velocity (9.43 km/s) such that the respective c.m. velocities were $u(CD_3^+) = 5.83$ km/s and $u(S) = 3.6$ km/s. This led to an estimate of the effective surface mass involved in the collision of $m(S)_{eff} = 29$ a.m.u., corresponding approximately to the mass of one terminal C_2H_5- group or two terminal CH_3- groups of surface hydrocarbons.

As in the earlier analyses of the CD_5^+ and CD_3^+ data, the scattering data from the $CD_4^{\bullet+}$ surface collisions were summarized in the simplified scattering diagram (data from Fig. 14). The scattering diagram for the product ions $CD_4^{\bullet+}$, CD_3^+ and CD_2H^+ from $CD_4^{\bullet+}$ collisions at 10.65 eV (Fig. 17) was considerably more complicated than those for CD_5^+ and CD_3^+ collisions. The data fell on two circles, one of which could be related to non-dissociative inelastic scattering of $CD_4^{\bullet+}$ (open circles) and direct dissociative scattering leading to the fragment CD_3^+ (open triangles at higher velocities and low scattering angles). The center of this circle bisected the relative velocity at a point CM(A) which suggested the effective mass of the surface involved in the inelastic scattering process of about 21 a.m.u. (between the mass of one terminal CH_3- and C_2H_5- group of the surface hydrocarbons). The data for CD_2H^+, one of the fragmentation products of surface chemical reaction (4b), together with lower-velocity data for CD_3^+ at small scattering angles and

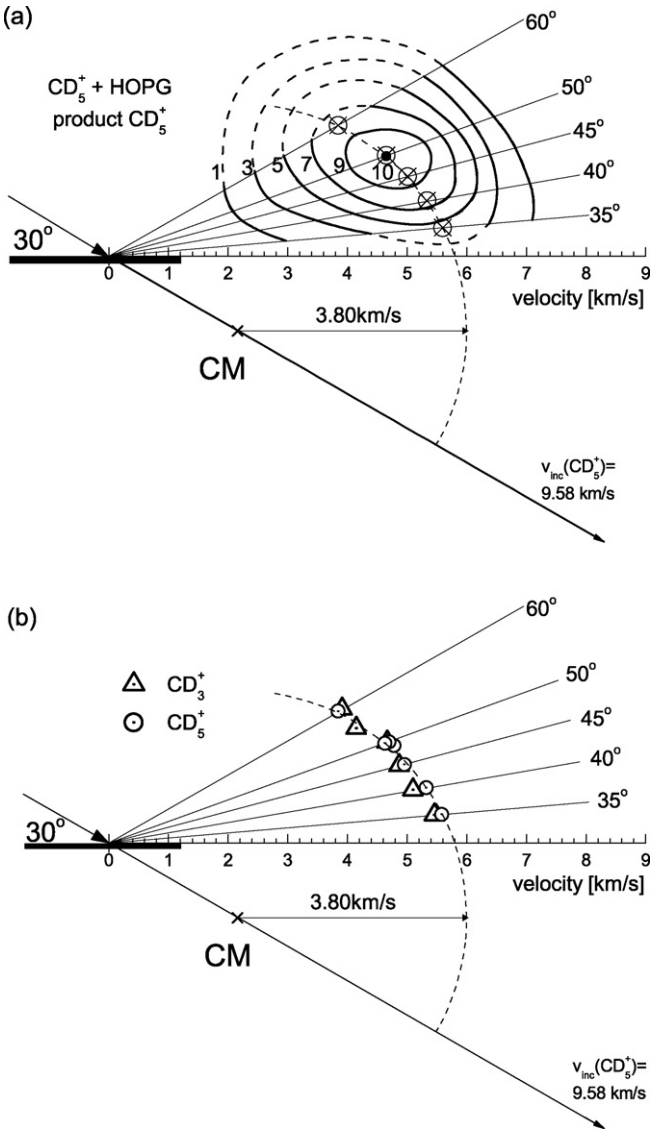

Fig. 15. Velocity scattering diagram of the product ion CD_5^+ from collisions of CD_5^+ at incident energy of 10.45 eV: (a) contour diagram of CD_5^+ and (b) simplified scattering diagram with velocity peak positions of product ions CD_5^+ and CD_3^+.

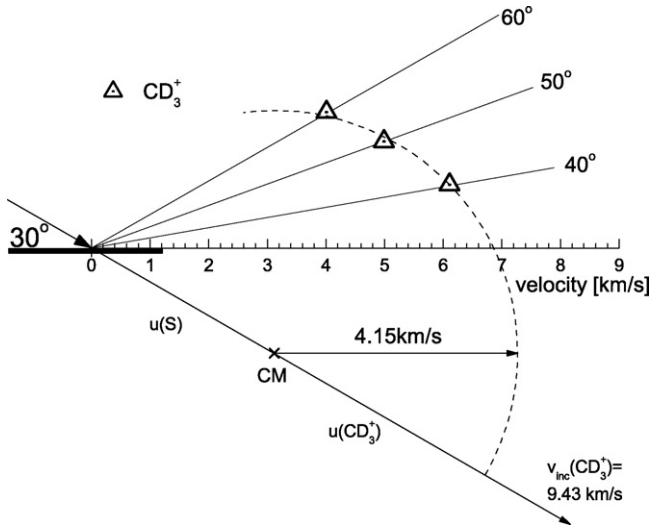

Fig. 16. Simplified velocity scattering diagram of product ions CD_3^+ from collisions of CD_3^+ at 8.3 eV.

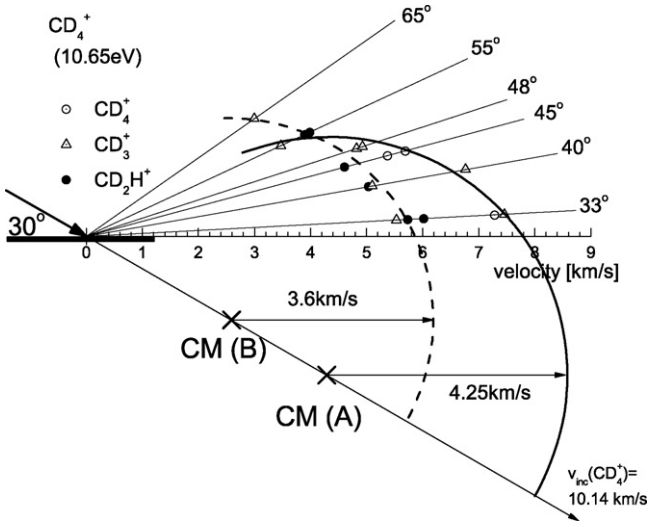

Fig. 17. Simplified velocity scattering diagram of the product ions $CD_4^{\bullet+}$, CD_3^+, and CD_2H^+ from collisions of CD_4^+ at 10.45 eV showing positions of peaks of velocity distributions.

CD_3^+ at large scattering angles, related evidently to the other fragmentation product of reaction (4), fitted well on a circle bisecting the relative velocity at CM(B). The above-mentioned estimation of the effective surface mass involved in this process led to a different effective mass of 48 a.m.u. This suggested that the mechanism of the chemical reaction of H-atom transfer was considerably more complicated than a simple direct H-atom pick-up reaction known from gas-phase ion–molecule reactions. (namely collision with a quasi-free hydrogen atom, see, e.g., [33] and references therein). By analogy with the gas phase, one would then expect the effective surface mass to be very small, approaching the mass of the transferred H-atom. The mechanism of hydrogen transfer reactions in low-energy polyatomic ion–hydrocarbon surface collisions was discussed earlier [34] and it was suggested that it involved projectile ion neutralization, sputtering of a proton from the surface, addition of the proton to the neutralized projectile, and mobile hydrogen atom surface recombination stabilizing the surface radicals formed.

Finally, scattering data for $CD_4^{\bullet+}$ and CD_3^+ at the incident energy of 5.6 eV, led to the scattering diagram in Fig. 18. Chemical reaction (4) was of little importance here (see Fig. 11b) and thus the data

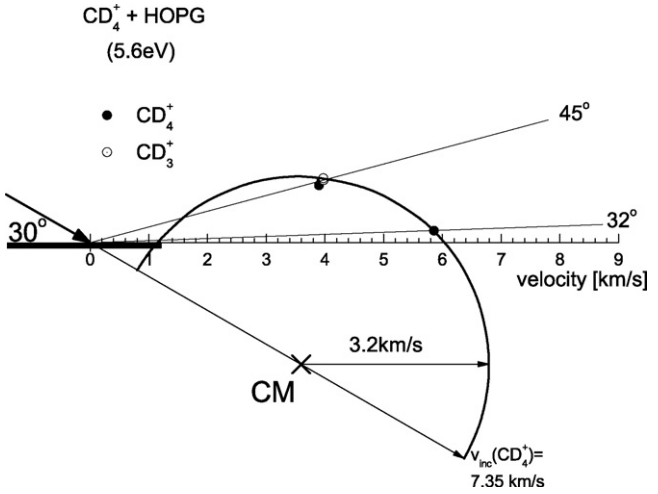

Fig. 18. Simplified velocity scattering diagram of $CD_4^{\bullet+}$ and CD_3^+ from collisions of $CD_4^{\bullet+}$ at 5.6 eV.

presumably refer only to non-dissociative and dissociative scattering of $CD_4^{\bullet+}$ and to a rough estimation of the effective surface mass of the surface of 15.4 a.m.u., corresponding to about the mass of one terminal CH_3– group of surface hydrocarbons, in reasonable agreement with the data at 10.65 eV for the inelastic scattering and direct fragmentation of CD_4^+ on the carbon surface.

4. Conclusions

1. Collisions of simple hydrocarbon ions CD_3^+, $CD_4^{\bullet+}$, CD_5^+ with very low incident energies in the range 3–10 eV and incident angle of 30° with room-temperature carbon (HOPG) surfaces were investigated in scattering experiments. Mass spectra, angular and translational energy distributions of product ions were determined.
2. The ion survival probability was about 12% for CD_5^+, and about 0.3–0.4% for CD_3^+ and $CD_4^{\bullet+}$ at 10 eV, decreasing towards zero with decreasing energy.
3. The product ions of CD_5^+ collisions were inelastically scattered CD_5^+ (peak energy at the angular maximum 30% of the incident energy) and CD_3^+ ions, the latter resulting from fragmentation of internally excited projectile ions. Kinematic analysis of the collisions at 10.45 eV led to an estimate of the effective mass of the surface involved in the collision of CD_5^+ of about 62 a.m.u. (comparable to the mass of a few CH_3– or C_2H_5– terminal groups of surface hydrocarbons).
4. Scattering of CD_3^+ led only to inelastically scattered CD_3^+ product, with about 30% of the incident energy (in the angular maximum). Kinematic analysis at 8.3 eV gave and estimate of the effective surface mass involved in the inelastic collision, $m(S)_{eff}$, of 29 a.m.u.
5. The incident radical cation $CD_4^{\bullet+}$ reacted with the hydrocarbon surface both in inelastic and fragmentation collisions (products $CD_4^{\bullet+}$ and CD_3^+) and in chemical reactions with surface hydrocarbons (H-atom transfer, and a small contribution of C-chain build-up reactions leading to C_2 hydrocarbon ions). The peak translational energy of the $CD_4^{\bullet+}$ in the angular maximum was again 30% of the incident energy. Kinematic analysis of the scattering gave for the effective mass of the surface involved in inelastic and direct dissociative collisions $m(S)_{eff}$ 15–21 a.m.u. at collision energies 5.9 and 10.65 eV, respectively (about one CH_3– group of surface hydrocarbons), but for the reactive scattering (formation of CD_4H^+ and its fragmentation products CD_2H^+ and CD_3^+) the estimated value of $m(S)_{eff}$ was 48 a.m.u., implying a more complicated surface process than a simple direct H-atom pick-up.

Acknowledgments

This research was partly supported by the Association EURATOM.IPP.CR in cooperation with Association EURATOM-ÖAW, by the I.A.E.A. under the Research Contract No. 13488, and by the Grant Agency of the Academy of Sciences (grant No. KAN400400651). F.Z. wishes to thank Association EURATOM-ÖAW for supporting his 2007 visit in the Prague laboratory.

References

[1] J.W. Rabalais (Ed.), Low Energy Ion–Surface Interactions, J. Wiley, New York, 1994.
[2] R.G. Cooks, T. Ast, Md.A. Mabud, Int. J. Mass Spectrom. 100 (1990) 209.
[3] L. Hanley (Ed.), Int. J. Mass Spectrom. 174 (1994) 1.
[4] V. Grill, J. Shen, C. Evans, R.G. Cooks, Rev. Sci. Instrum. 72 (2001) 3149.
[5] W.O. Hofer, J. Roth (Eds.), Physical Processes of the Interaction of Fusion Plasmas with Solids, Academic Press, San Diego, CA, 1996.
[6] Z. Herman, J. Am. Soc. Mass Spectrom. 14 (2003) 1360.
[7] V.H. Wysocki, J.L. Jones, J.M. Ding, J. Am. Chem. Soc. 113 (1991) 8969.

[8] B.E. Winger, R.K. Julian, R.G. Cooks, C.E.D. Chidsey, J. Am. Chem. Soc. 113 (1991) 8967.
[9] J. Laskin, E. Denisov, J.H. Futrell, J. Phys. Chem. B 105 (2001) 1895.
[10] R.G. Cooks, J.W. Amy, M.E. Bier, J.C. Schwarz, K.L. Schey, Adv. Mass Spectrom. 11 (1989) 33.
[11] A.L. McCormack, J.L. Jones, V.H. Wysocki, J. Am. Soc. Mass Spectrom. 3 (1992) 859.
[12] A.L. Mc Cormack, A. Somogyi, A.R. Dongre, V.H. Wysocki, Anal. Chem. 65 (1993) 2859.
[13] S. Rakov, E. Denisov, J. Laskin, J.H. Futrell, J. Phys. Chem. A 106 (2002) 2781.
[14] J. Alvarez, J.H. Futrell, J. Laskin, J. Phys. Chem. A 110 (2006) 1678.
[15] C.M. Jones, R.L. Beardsley, A.S. Gelhena, S. Dagan, G. Cheng, V.H. Wysocki, J. Am. Chem. Soc. 128 (2006) 15044.
[16] J. Laskin, J.H. Futrell, J. Chem. Phys. 119 (2003) 3413.
[17] O. Meroueh, W.L. Hase, J. Am. Chem. Soc. 124 (2002) 1524.
[18] E. Martinez-Nunez, A. Rahaman, W.L. Hase, J. Phys. Chem. C 111 (2007) 354.
[19] J. Kubišta, Z. Dolejšek, Z. Herman, Eur. Mass Spectrom. 4 (1998) 311.
[20] J. Žabka, Z. Dolejšek, Z. Herman, J. Phys. Chem. A 106 (2002) 10861.
[21] J. Roithová, J. Žabka, Z. Dolejšek, Z. Herman, J. Phys. Chem. B 106 (2002) 8293.
[22] J. Žabka, Z. Dolejšek, J. Roithová, V. Grill, T.D. Märk, Z. Herman, Int. J. Mass Spectrom. 213 (2002) 145.
[23] J. Jašík, J. Žabka, L. Feketeová, I. Ipolyi, T.D. Märk, Z. Herman, J. Phys. Chem. A 109 (2005) 10208.
[24] J. Jašík, J. Roithová, J. Žabka, A. Pysanenko, L. Feketeová, I. Ipolyi, T.D. Märk, Z. Herman, Int. J. Mass Spectrom. 249/250 (2006) 162.
[25] A. Somogyi, D.L. Smith, V.H. Wysocki, R. Colorado, T.R. Lee, J. Am. Soc. Mass Spectrom. 13 (2002) 1151.
[26] B. Rasul, F. Zappa, N. Endstrasser, W. Schustereder, J.D. Skalny, Z. Herman, P. Scheier, T.D. Märk, 18th International Conference on Plasma–Surface Interactions, Toledo (E), 2008 (Abstracts of papers).
[27] S.G. Lias, J.E. Bartmess, J.F. Liebman, J.L. Holmes, R.D. Levine, W.G. Mallard, J. Phys. Chem. Ref. Data 17 (Suppl. 1) (1988).
[28] J. Glosík, V. Skalský, C. Praxmarer, D. Smith, W. Freysinger, W. Lindinger, J. Chem. Phys. 101 (1994) 3792.
[29] A. Qayyum, T. Tepnual, C. Mair, S. Matt-Leubner, P. Scheier, Z. Herman, T.D. Mark, Chem. Phys. Lett. 376 (2003) 539.
[30] D.J. Garton, T.K. Minton, M. Alagia, N. Balucani, P. Casavecchia, G.G. Volpi, J. Chem. Phys. 112 (2000) 5975.
[31] J. Zhang, D.J. Garton, T.K. Minton, J. Chem. Phys. 117 (2002) 6239.
[32] B. Friedrich, Z. Herman, Collect. Czech. Chem. Commun. 49 (1984) 570.
[33] Z. Herman, Int. J. Mass Spectrom. 212 (2001) 413.
[34] L.M. Phelan, M.J. Hayward, J.C. Flynn, S.L. Bernasek, J. Phys. Chem. B 102 (1998) 5667.